Pin Fin Heat Sink Performance

Under Air Jet Impingement

Jet impingement is one of the most efficient methods of cooling hot electronic devices, as it can create a very high heat transfer rate on an impacting surface. As the power density of modern chips keeps increasing, using air jet impingement to remove heat from a heat sink or electronic components has been employed on numerous applications. The most common example is the fan sink with a fan mounted on top of heat sink to create air jets.

Experimental and numerical investigations of flow and heat transfer characteristics under single or multiple impinging jets remain a very dynamic research area in the past two decades. For cooling of high power devices, there are many publications about the heat transfer mechanism of single or multiple free-surface, submerged and confined jets. But, in real electronics cooling applications, fan sinks with a single fan are most commonly used to cool the high-power devices on a PCB board. There has been a lot of research on how to optimize the heat sink design under air jet impingement to achieve lower thermal resistance with limited pumping power.

El-Sheikh and Garimella [1] conducted air jet impingement tests by using a variety of pin-fin heat sinks mounted on a heat source. They tried to find a way to optimize the heat sink performance by varying pin fin the dimensions and air jet configurations. The test apparatus El-Sheikh and Garimella devised is illustrated in Figure 1.

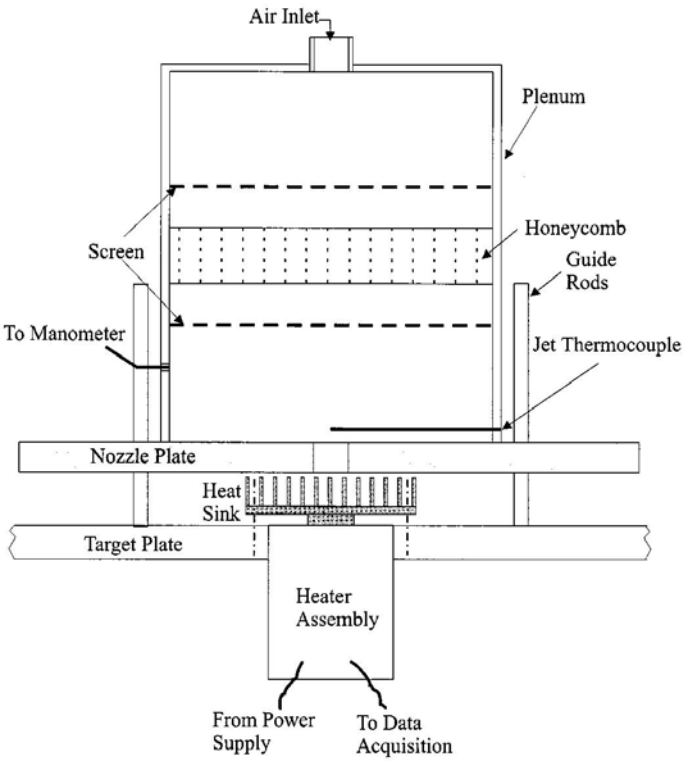

Figure 1. Schematic of the Air Jet Impingement Test Section [1]

The heat sink was mounted on a square heat source (20 x 20 mm). An orifice on a nozzle plate installed above the heat sink was used to create the air jet. A pressure tap located on the plenum wall is used to measure pressure drop across the orifice, while a thermocouple measures the air temperature just upstream of the orifice. The nozzle-to-target plate spacing is set using three small high-precision gage blocks. Three different orifice plates were used in the experiments, with square-edged orifices of diameters of 12.7, 25.4, and 38.1 mm.

Seven copper pin-fin heat sinks were studied in the experiments by El-Sheikh and Garimella. The dimensions of these heat sinks are listed in Table 1. Two sizes of heat sink footprint were considered: Small (50.8 x 50.8 mm) and Large (76.2 x 76.2 mm). The thickness of the heat sink base was held at 3.17 mm for all heat sinks. Pin fins of a diameter of 1.6 mm were studied at pin heights of 12.7 and 25.4 mm. A smaller pin diameter, 0.94 mm, was also considered. Two unpinned heat sinks with smooth bases were studied as a baseline benchmark. To compare the heat sinks with pin and without pins, the average heat transfer coefficient h_{base} for the heat sinks was calculated according to

$$h_{base} = \frac{Q_{tot} - Q_{loss}}{A_{base}\,(T_{base} - T_{jet})}$$

Where Q_{tot} is overall heat flux, Q_{loss} is heat loss to ambient, A_{base} is heat sink base area.

Figure 2 shows the heat sink assembly, heater section and nozzle nomenclature. For small heat sinks, the measured average heat transfer coefficients of two different pin heights, and unpinned case for different nozzle sizes, are shown in Figure 3. In all cases, the heat transfer coefficient is seen to increase as the nozzle diameter decreases at a fixed flow rate. The influence of nozzle diameter is much more pronounced for the unpinned heat sink than for the pinned sinks. However, El-Sheikh and Garimella think that this trend may not continue to be valid for nozzle diameters outside the range considered here; for instance, if much smaller diameters were used, the ratio of target surface area to the nozzle open area would be greatly increased, and the average heat transfer for a fixed target area may decrease with a decrease in nozzle diameter. And the pined heat sinks have much large average heat transfer coefficients than the unpinned heat sink due to increased surface area.

	Description	Base footprint, A_{base} (mm x mm)	Effective Surface area[§], A_{HS} (10^{-4} m^2)	Pin height, H_p (mm)	Pin diameter, d_p (mm)	Number of Pins	Pin Spacing (mm)	Pin Arrangement
Large pinned heat sinks (76.2x76.2 mm^2 footprint)	Short	76.2x76.2	371	12.7	1.6	540	2.9	Staggered
	Tall	76.2x76.2	747	25.4	1.6	540	2.9	Staggered
Small pinned heat sinks (50.8x50.8 mm^2 footprint)	Short	50.8x50.8	179	12.7	1.6	240	2.9	Staggered
	Short, fine pins	50.8x50.8	201	12.7	0.94	480	2.28	Staggered
	Tall	50.8x50.8	332	25.4	1.6	240	2.9	Staggered
Unpinned heat sinks (both footprints)	Large	76.2x76.2	58	0	-	0	0	N/A
	Small	50.8x50.8	26	0	-	0	0	N/A

[§] Includes surface area of pins and remaining footprint area of the base; i.e., side and bottom surface of the base not included.

Table 1. Heat Sink Dimension [1]

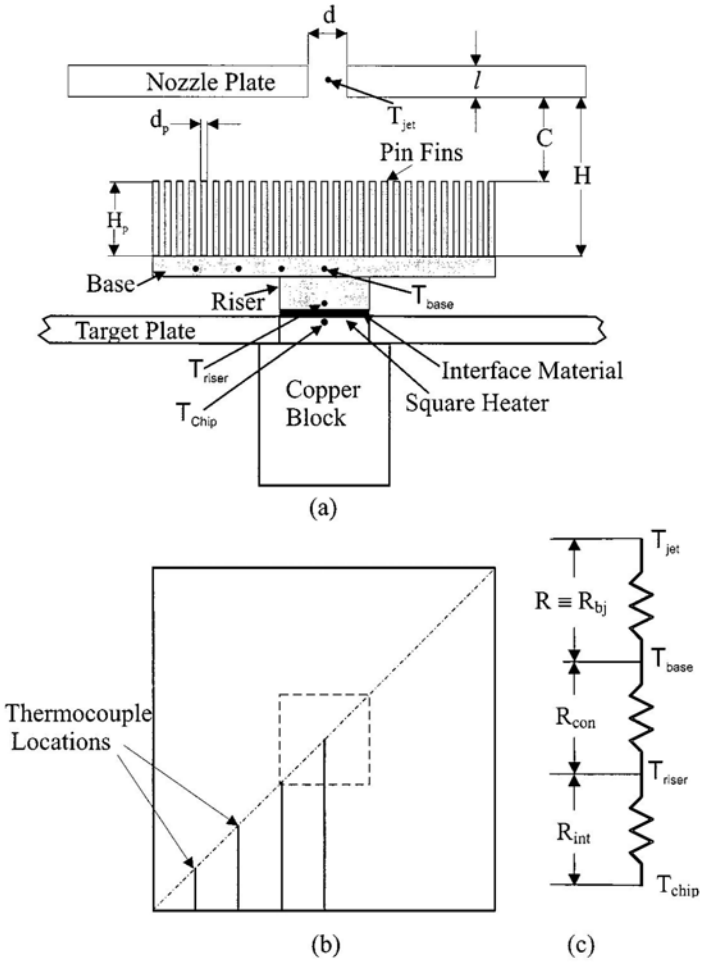

Figure 2. (a) Pin fin Heat Sink Geometric Parameters, (b) Top View of the Heat Sink Base with Thermocouple Locations, and (c) Thermal Resistance Diagram

Similar results for the unpinned and pinned large heat sinks are shown in Figure 4. As for the small heat sink, the heat transfer coefficient increases as nozzle diameter decreases, especially for the unpinned heat sink. However, the influence of nozzle diameter almost entirely vanishes for the taller pinned heat sink. El-Sheikh and Garimella concluded that the key factors governing heat transfer rates in confined jet impingement on heat sinks are the jet exit velocity and the total surface area of the heat sink. It may be inferred from the results that as the heat sink surface area is increased, a critical value is reached beyond which it overshadows the role of jet velocity. Thus, for the relatively large surface areas characterizing the large pinned heat sinks, changes in the nozzle diameter at a fixed flow rate have little or no effect on heat transfer, as demonstrated in Figure 4.

El-Sheikh and Garimella also found that increasing the surface area of a heat sink with a given footprint, by increasing the height of the pins, leads to only modest gains in heat transfer coefficient. This is illustrated in Figure 5, where the effect of pin height is investigated for the small and large heat sinks, for a fixed nozzle diameter of 12.7 mm. Two effects come into play in these results. On the one hand, the fin efficiency of each pin decreases as the pin height increases. However, since the pin fins in this study are made of copper, they retain most of the fin efficiency, even as the pin height is increased from 12.7 mm to 25.4 mm, with the efficiency reducing from 98% to 80%. A second and more important effect is related to the details of the impingement flow field: the increase in pin height adds area in a region of low flow velocities and, hence, does not add perceptibly to heat transfer. Thus, although the taller-pin heat sinks comprise almost twice the area of the shorter-pin counterparts, the heat transfer coefficients are only different by 5%. This is true for both the small and large heat sinks.

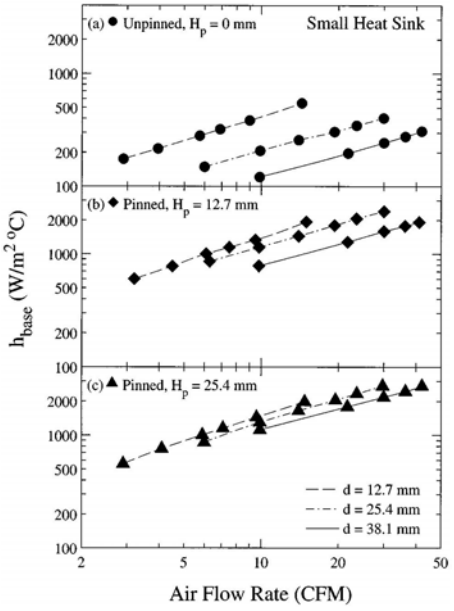

Figure 3. Small Heat Sinks Heat Transfer Coefficient as a Function of Air Flow Rate with Different Nozzle Diameters and C=12.7 mm [1]

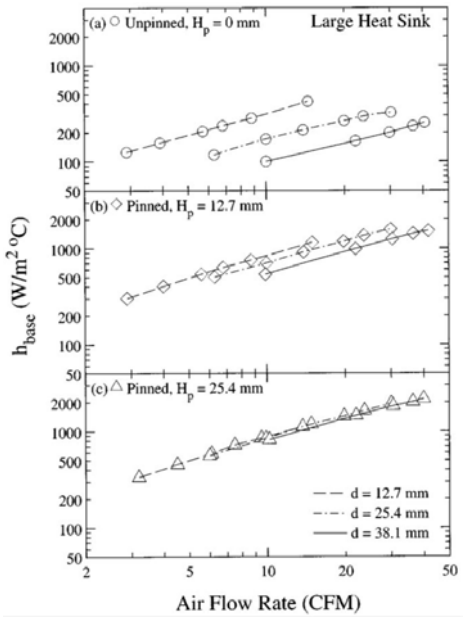

Figure 4. Large Heat Sinks Heat Transfer Coefficient as a Function of Air Flow Rate with Different Nozzle Diameters and C=12.7 mm [1]

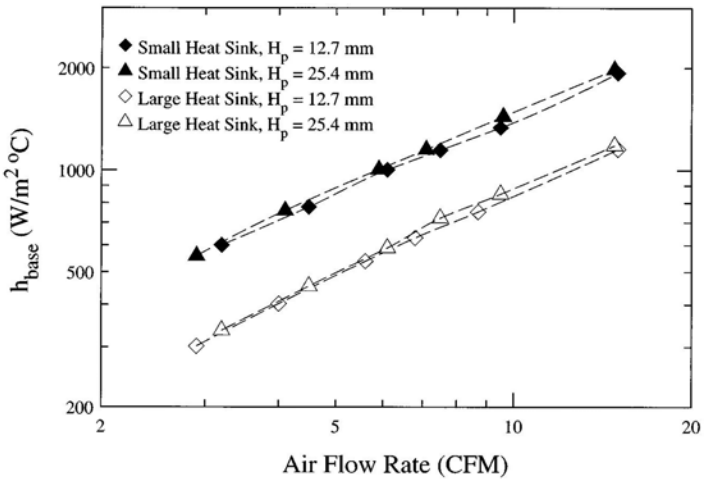

Figure 5. Heat Transfer Coefficient as a Function of Air Flow Rate for the Small and Large Heat Sinks at Two Different Pin Heights, for d=12.7 mm

El-Sheikh and Garimella also measured the pressure drop from nozzle to ambient. They found the pressure drop strongly depends on jet speed. Most of the pressure drop in this cooling technique occurs across the nozzle; the nozzle pressure drop overwhelms any contribution of the presence of the heat sink to pressure drop. Clearly, decreasing the nozzle size will cause large pressure drop increase.

By analyzing their test results, El-Sheikh and Garimella concluded that a decrease in nozzle diameter resulted in an improvement in heat transfer for a fixed flow rate. However, the effect of nozzle diameter was much more pronounced for the unpinned heat sinks. The competing effects of jet velocity and heat sink surface area, in determining the heat transfer from the heat sink, need to be considered when designing a jet impingement cooled heat sink.

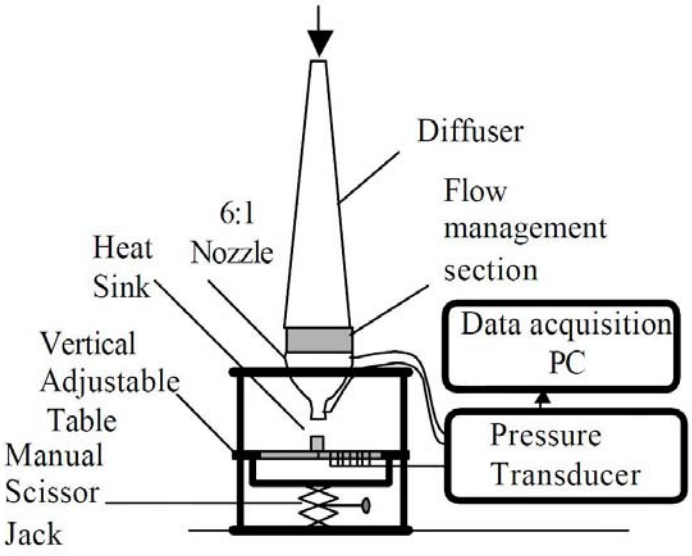

Figure 6. Schematic of Jet Impingement Experiment Setup [2]

Issa and Ortega [2] experimentally investigated flow behavior, pressure drop and heat transfer of square pin fin heat sinks under free air jet impingement. Their test setup is illustrated in Figures 6 and 7. A 6:1 contracting nozzle has an exit with cross-section areas of 25 mm x 25 mm, which creates a uniform air jet. Test heat sink (25 mm x 25 mm, L x W) is located directly under the nozzle exit. A 25 mm x 25 mm Kapton surface heater is placed underneath the heat sink to supply the heat. The heat sink base and heater are insulated by a Renshape block. The heat sinks they tested are listed in Table 2. The heat sink thermal resistance is calculated based on the following equation,

$$R = \frac{T_{base} - T_{jet}}{Q_{tot} - Q_{loss}}$$

In the test, the jet Reynolds Number is defined as,

$$Re = \frac{\rho \cdot V \cdot W}{\mu}$$

Where W is heat sink and nozzle exit width.

Figure 8 shows the measure thermal resistance for heat sinks 1C, 2C and 3C (H=22.5mm) with zero jet clearance. The three heat sinks have different numbers of fins, but share the same fin height. Clearly, the heat sink thermal resistance decreases monotonically with increase of jet velocity (Reynolds Number). And, a heat sink with more fins (more surface area) has a smaller thermal resistance.

Figure 9 shows the measured thermal resistance for heat sinks 1A, 1B and 3C (8X8 fins) with zero jet clearance. The three heat sinks have the same number of fins but different fin heights. At low jet velocity (Reynolds Number), a heat sink with taller fins has a smaller thermal resistance. But, as

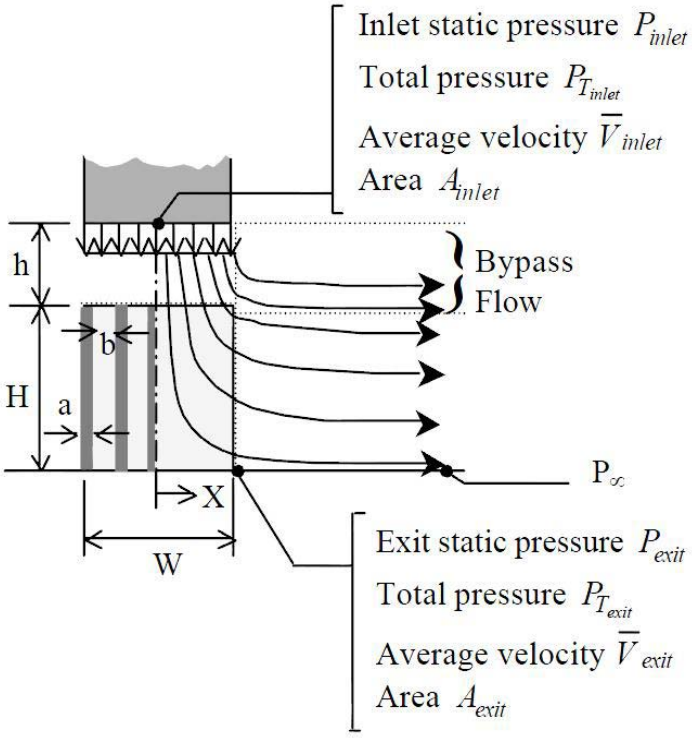

Figure 7. Test Section and Heat Sink Dimension [2]

Desc.	*a*	*b*	*H*	*n*	*a/H*	*b/a*	*H/W*
1A	1.5	1.86	12.5	8	0.12	1.24	0.5
1B	1.5	1.86	17.5	8	0.09	1.24	0.7
1C	1.5	1.86	22.5	8	0.07	1.24	0.9
2A	1.5	2.42	12.5	7	0.12	1.61	0.5
2B	1.5	2.42	17.5	7	0.09	1.61	0.7
2C	1.5	2.42	22.5	7	0.07	1.61	0.9
3A	1.5	3.2	12.5	6	0.12	2.13	0.5
3B	1.5	3.2	17.5	6	0.09	2.13	0.7
3C	1.5	3.2	22.5	6	0.07	2.13	0.9
4A	1.5	4.38	12.5	5	0.12	2.92	0.5
4B	1.5	4.38	17.5	5	0.09	2.92	0.7
4C	1.5	4.38	22.5	5	0.07	2.92	0.9
5A	1.5	6.33	12.5	4	0.12	4.22	0.5
5B	1.5	6.33	17.5	4	0.09	4.22	0.7
6A	2	3.75	12.5	5	0.16	1.88	0.5
6B	2	3.75	17.5	5	0.11	1.88	0.7
6C	2	3.75	22.5	5	0.09	1.88	0.9
7A	2.5	3.13	12.5	5	0.20	1.25	0.5
7B	2.5	3.13	17.5	5	0.14	1.25	0.7
7C	2.5	3.13	22.5	5	0.11	1.25	0.9

Table 2. Heat Sinks Geometries (All Dimensions in mm) [2]

the jet velocity increases, the thermal resistance discrepancy between heat sinks with different fin heights almost disappears. Figure 10 illustrates the same trend for other heat sinks.

Figure 11 shows the effect of the clearance ratio on thermal resistance for heat sinks 1A, 1B and 3C (8X8 fins). For each heat sink, the thermal resistance increases with an increase of the clearance ratio. This is understandable, because the jet covers the whole heat sink. When clearance ratio increases, some flow bypasses the heat sink, which results in less cooling of the heat sink. However, the overall pressure drop would be less, due to the flow bypass.

Issa and Ortega also measured the pressure drop across the heat sink. They found that the pressure loss coefficient shows little dependence on the Reynolds Number. This may be because the flow is in a fully turbulent regime. At a fixed jet speed, the pressure drop increased with the increase of pin density and pin diameter, and decreased with increased pin height. Also, pressure drop decreases rapidly with an increase of tip clearance, with most of the reduction occurring within clearance ratios up to 25%.

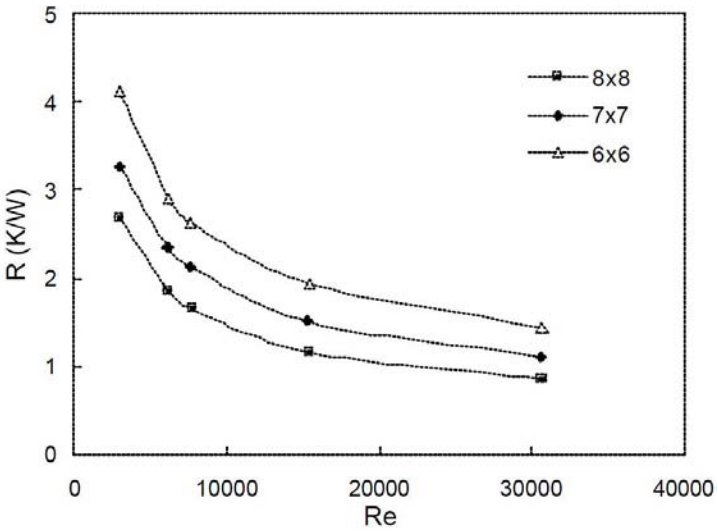

Figure 8. Heat Sink Thermal Resistance Dependence on Reynolds Number at h/H=0 for 1C, 2C, and 3C [2]

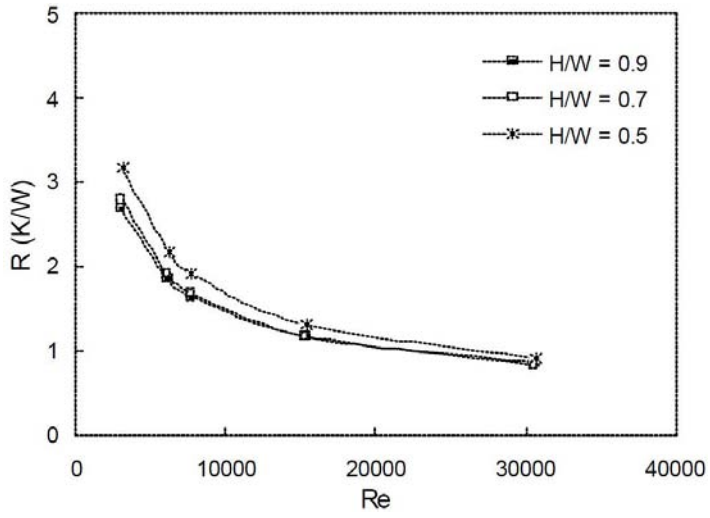

Figure 9. Heat Sink Thermal Resistance vs. Reynolds Number at h/H=0, for 1A, 1B and 1C (8x8) [2]

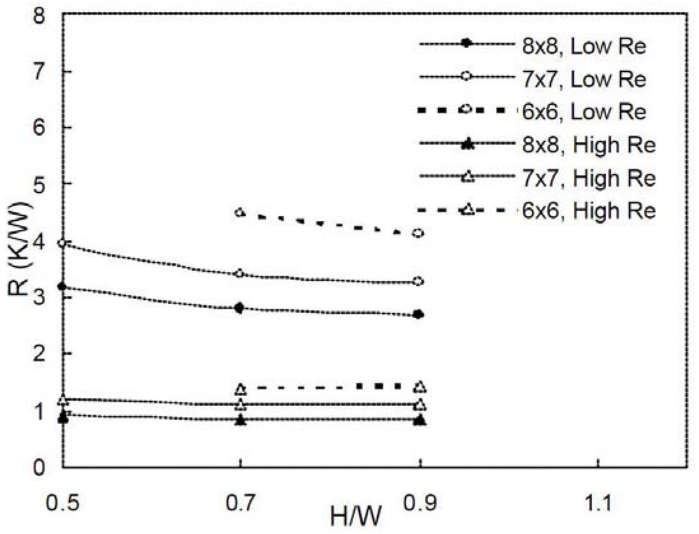

Figure 10. Heat Sink Thermal Resistance vs. Pin Height at High Re=30600 and Low Re=3000 with h/H=0 [2]

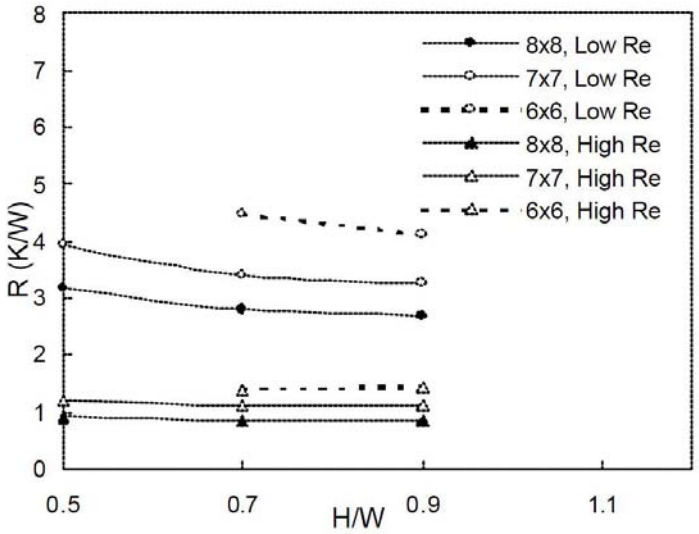

Figure 11. Heat Sink Thermal Resistance vs. Clearance Ratio at High Re=30600 and Low Re=3000 for 1A, 1B and 1C (8x8) [2]

For the thermal test, Issa and Ortega found that the heat sink thermal resistance decreases with increasing jet speed, pin density and pin diameter. They noticed that the thermal resistance is weakly dependent on pin height at high jet speed. Also, at high jet speed, the heat sink thermal resistance is not sensitive to the tip clearance ratio.

This paper summarizes the research on pin fin heat sinks under single confined jets, conducted by El-Sheikh and Garimella [1], and the study of pin fin heat sinks under single free jets, completed by Issa and Ortega [2]. Their experimental tests shows that the thermal performance of pin fin heat sinks behave similarly under some circumstances and act differently under some other configurations for confined jet impingement and free jet impingement. In conclusion, engineers have to be careful about the details of the pin fin heat sink design, configuration and its implementation when they use jet impingement as a cooling method.

References:

1. **El-Sheikh, H. A., and Garimella, S. V., "Enhancement of Air Jet Impingement Heat Transfer Using Pin-Fin Heat Sinks", IEEE Transactions on Components and Packaging Technology, VOL. 23, NO. 2, June 2000.**

2. **Issa, J. S., and Ortega, A., "Experimental Measurements of the Flow and Heat Transfer of a Square Jet Impinging on an Array of Square Pin Fins", Proceedings of ASME International Engineering Congress & Exposition, November 17-22, 2002, New Orleans, Louisiana.**